Comprehensive study of endurance for IAR-99 Hawk

Dorin LOZICI-BRINZEI*,[1], Simion TATARU[2], Radu BISCA[1], Daniela BARAN[1]

*Corresponding author
*,[1]INCAS – National Institute for Aerospace Research "Elie Carafoli"
B-dul Iuliu Maniu 220, Bucharest 061126, Romania
lozicid@incas.ro*, biscar@incas.ro, dbaran@incas.ro
[2]Aerospace Consulting
B-dul Iuliu Maniu 220, Bucharest 061126 Bucharest, Romania
sitataru@incas.ro

DOI: 10.13111/2066-8201.2014.6.1.6

Abstract: *The paper presents some methods of on-ground and in-flight calibration for strain gauges, intended to the development of complex programs which analyze the endurance phenomena for aerospace structures, with direct application to the IAR-99 Hawk. The strain gauges have the advantage of being sensitive to load and therefore to aerodynamic phenomena, thereby providing indications of the loads supported by the structure. The effects size of loads type phenomena caused by wind gusts or buffet can be measured only by strain gauges or accelerometres[70] and they cannot be recorded by flight or fatigue parameters counters. The installation of a strain gauge is made using a pattern (its position and orientation are crucial) and the strain gauge selected for installation should not be fragile or unstable. Routines should be established for periodic inspection of strain gauges and those which are defective should be replaced immediately.*

Key Words: *aerospace structures, fatigue parameters, strain gauges, calibration, test benchmark*

1. INTRODUCTION

The paper presents some methods of on- ground and in-flight calibration for strain gauges, intended to the development of complex programs which analyze the endurance phenomena for aerospace structures, with direct application to the IAR-99 Hawk. As the fatigue wear of the military aircraft is usually correlated to defects accumulated on a wear tested benchmark, the calibration of the strain gauges positioned in locations similar to those of the benchmark test is essential to obtain accurate estimates of the reserve of fatigue strength Strain gauges must be calibrated so that loads determined based on their signals can be directly compared with those of the fatigue test benchmark. To check the test load, strain gauges on test benchmark can be calibrated according to the answer of some strain gauges mounted on the aircraft specially equipped for the load study. Furthermore, two strain gauges placed at nominally identical locations, but on two different airplane structures, may have slightly different answers due to small differences in the quality of construction of the structure, alignment of strain gauges, thickness of adhesive used and the scale factor or the sensitivity of the strain gauge / amplifier. More paths to load a redundant structure can also cause variable strain gauge responses resulting from the differences already existing before the delivery into the structure. The calibration is also necessary to consider the zero drift of the strain gauge. The analytical prediction of the calibration factor should be adopted because it is very expensive to make a ground calibration for each airplane. Although the fleet of about

20 IAR-99 aircraft is relatively small, the financial effort to calibrate each aircraft would be a major one. For this reason, analytical methods, involving the identification of the STIP and similar configurations have been developed and validated by on-ground calibration of several aircraft from different squadrons. On-ground calibration involved the application of distributed or lumped loads to the structure in question and the simultaneous recording of the response of the strain gauges mounted on the structure. This procedure was used to identify the loads for the bending moment of the wing embedding (by regression) for wings, vertical empennages and horizontal stabilizers in order to validate the analytical method. Alternatively, the strain gauges can be calibrated in-flight, in certain configurations and regimes that are often used. For instance, the 1g condition with standard weight and external stores could be used. The main advantage of this method is that it can be automated to reduce the effort of the data post-processing.

2. CALIBRATION OF THE STRAIN GAUGES FOR IN-FLIGHT MEASURING OF LOADS

Figure 1 shows an outline of the IAR-99 aircraft wing in the embedding area. The wing has a classical structure with two spars, webs and flanges that were instrumented with two rosettes (8 simple strain gauges disposed in a *cross-like* configuration) and 8 simple stretch-compression stain gauges.

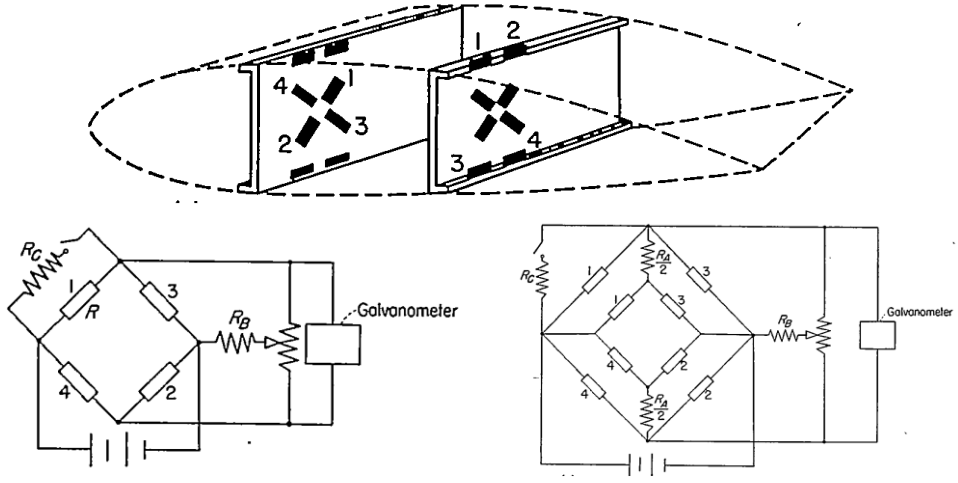

Figure 1 Typical ways of strain gauges installation

For a wing whose structure satisfies Hooke's law, three terms can be considered to describe a simplified equation of shear, bending and torsion loads. The relationship between the "μ" output of the strain gauge and the loads (shear, bending and torque moment) can be expressed by the equation:

$$\mu_i = \alpha_{i1} V + \alpha_{i2} M + \alpha_{i3} T \tag{1}$$

$$\begin{aligned} M &= V_y \\ T &= V_x \end{aligned} \tag{2}$$

$$\frac{\mu_i}{V} = \alpha_{i1} + \alpha_{i2} y + \alpha_{i3} x \tag{3}$$

Equation (3) shows that the strain gauge output is proportional to the V shear and the relationship between this output and the application point coordinates (x, y) is linear.

$$\mu_i = \alpha_{i1}V + \alpha_{i2}V_y + \alpha_{i3}V_x + \alpha_{i4}V_{xy} + \alpha_{i5}Vx^3 + \alpha_{i6}Vy^2 + \cdots \alpha_{ij}Vx^r y^s \tag{4}$$

An extension of equation (3) which includes additional terms has the form of equation (4)

$$\left.\begin{array}{l} \mu_1 = \alpha_{11}V + \alpha_{12}V_y + \alpha_{13}V_x + \cdots \alpha_{1j}Vx^r y^s \\ \mu_2 = \alpha_{21}V + \alpha_{22}V_y + \alpha_{23}V_x + \cdots \alpha_{2j}Vx^r y^s \\ \mu_3 = \alpha_{31}V + \alpha_{32}V_y + \alpha_{33}V_x + \cdots \alpha_{3j}Vx^r y^s \\ \ldots\ldots\ldots\ldots\ldots\ldots\ldots\ldots\ldots\ldots\ldots\ldots\ldots\ldots\ldots\ldots\ldots\ldots\ldots\ldots \\ \ldots\ldots\ldots\ldots\ldots\ldots\ldots\ldots\ldots\ldots\ldots\ldots\ldots\ldots\ldots\ldots\ldots\ldots\ldots\ldots \\ \ldots\ldots\ldots\ldots\ldots\ldots\ldots\ldots\ldots\ldots\ldots\ldots\ldots\ldots\ldots\ldots\ldots\ldots\ldots\ldots \\ \mu_j = \alpha_{j1}V + \alpha_{j2}V_y + \alpha_{j3}V_x + \cdots \alpha_{jj}Vx^r y^s \end{array}\right\} \tag{5a}$$

These equations are expressed in a matrix form as:

$$\begin{Bmatrix} \mu_1 \\ \mu_2 \\ \mu_2 \\ . \\ . \\ . \\ \mu_j \end{Bmatrix} = \begin{bmatrix} \alpha_{11}\alpha_{12}\alpha_{13}\ldots\alpha_{1j} \\ \alpha_{21}\alpha_{22}\alpha_{23}\ldots\alpha_{2j} \\ \alpha_{31}\alpha_{32}\alpha_{33}\ldots\alpha_{3j} \\ \ldots\ldots\ldots\ldots \\ \ldots\ldots\ldots\ldots \\ \ldots\ldots\ldots\ldots \\ \alpha_{j1}\alpha_{j2}\alpha_{j3}\ldots\alpha_{jj} \end{bmatrix} \begin{Bmatrix} V \\ V_y \\ V_x \\ . \\ . \\ . \\ V_{x^r y^s} \end{Bmatrix} \tag{5b}$$

or

$$\{\mu\} = \{V_{x^r y^s}\} \tag{5c}$$

$$\{V_{x^r y^s}\} = [\beta]\{\mu\} \tag{6}$$

$$[\beta]=[\alpha]^{-1} \tag{7}$$

The necessary mathematical condition for the existence of a solution for the ß coefficients of equation (6) is that the determinant of the α equations coefficients (5) shall not vanish, that is

$$|[\alpha]| \neq 0 \tag{8}$$

$$\begin{Bmatrix} V \\ M \\ T \end{Bmatrix} = \left\| \begin{matrix} \beta_{11}\beta_{12}\beta_{13}\ldots\beta_{1j} \\ \beta_{21}\beta_{22}\beta_{23}\ldots\beta_{2j} \\ \beta_{31}\beta_{32}\beta_{33}\ldots\beta_{3j} \end{matrix} \right\| \begin{Bmatrix} \mu_1 \\ \mu_2 \\ \mu_2 \\ . \\ . \\ . \\ \mu_j \end{Bmatrix} \tag{9}$$

If these coefficients can be determined, then equation (9) can be used to determine the in-flight loads and the strain gauges response.

$$V = \begin{bmatrix} \beta_{11}\beta_{12}\beta_{13} & \ldots & \beta_{1j} \end{bmatrix} \begin{Bmatrix} \mu_1 \\ \mu_2 \\ \mu_2 \\ . \\ . \\ . \\ \mu_j \end{Bmatrix} \tag{10a}$$

or

$$V = \lfloor \mu_1 \mu_2 \mu_3 \ldots \mu_j \rfloor \begin{Bmatrix} \beta_{11} \\ \beta_{12} \\ \beta_{13} \\ . \\ . \\ . \\ \beta_{1j} \end{Bmatrix} \tag{10b}$$

$$\begin{Bmatrix} V_1' \\ V_2' \\ . \\ . \\ . \\ V_j' \end{Bmatrix} = \begin{bmatrix} \mu_{11}\mu_{12} \ldots \mu_{1j} \\ \mu_{21}\mu_{22} \ldots \mu_{2j} \\ \ldots \ldots \ldots \\ \ldots \ldots \ldots \\ \ldots \ldots \ldots \\ \mu_{j1}\mu_{j2} \ldots \mu_{jj} \end{bmatrix} \begin{Bmatrix} \beta_{11} \\ \beta_{12} \\ . \\ . \\ . \\ \beta_{1j} \end{Bmatrix} \tag{11a}$$

$$\{V'\} = [\mu]\{\beta\} \tag{11b}$$

$$\{\beta\} = [\mu]^{-1}\{V'\} \tag{12}$$

$$\begin{Bmatrix} V_1' \\ V_2' \\ . \\ . \\ . \\ V_j' \end{Bmatrix} = \left\| \begin{matrix} \mu_{11}\mu_{12} \ldots \mu_{1j} \\ \mu_{21}\mu_{22} \ldots \mu_{2j} \\ \ldots \ldots \ldots \\ \ldots \ldots \ldots \\ \ldots \ldots \ldots \\ \mu_{j1}\mu_{j2} \ldots \mu_{jj} \end{matrix} \right\| \begin{Bmatrix} \beta_{11} \\ \beta_{12} \\ . \\ . \\ . \\ \beta_{1j} \end{Bmatrix} \tag{13a}$$

or

$$\{V_n'\} = \|\mu_{nj}\|\{\beta_{1j}\} \tag{13b}$$

$$\left\{\|\mu_{nj}\|^T\{V_n'\}\right\} = \left[\|\mu_{nj}\|^T\|\mu_{nj}\|\right]\{\beta_{1j}\} \tag{14}$$

$$\{\beta_{1j}\} = \left[\|\mu_{nj}\|^T\|\mu_{nj}\|\right]^{-1}\left\{\|\mu_{nj}\|^T\{V_n'\}\right\} \tag{15}$$

The necessary condition for the existence of the least squares solution (15) in equation (14) is that the determinant of the matrix of normal equations be greater than zero.

$$\left|\left[\|\mu_{nj}\|^T\|\mu_{nj}\|\right]\right| > 0 \tag{16}$$

$$\{\epsilon_V\} = \{V\} - \{V'\} \tag{17}$$

$$P.E.(V) = 0.6745\sqrt{\frac{\sum \epsilon_{V^2}}{n-(q+1)}} \tag{18}$$

$$P\sum \epsilon_{V^2} = \sum (V'n)^2 - \lfloor \beta_{1j} \rfloor \left\{\|\mu_{nj}\|^T\{V'n\}\right\} \tag{19}$$

$$\begin{bmatrix} m_{11} & m_{12} & . & . & . & m_{1j} \\ m_{21} & m_{22} & . & . & . & m_{2j} \\ \vdots & \vdots & \vdots & \vdots & \vdots & \vdots \\ . & . & . & . & . & . \\ m_{j1} & m_{j2} & . & . & . & m_{jj} \end{bmatrix} = \left[\left\| \mu_{nj} \right\|^T \left\| \mu_{nj} \right\| \right]^{-1} \tag{20}$$

$$\begin{Bmatrix} P.E.(\beta_{11}) \\ P.E.(\beta_{12}) \\ . \\ . \\ . \\ P.E.(\beta_{1j}) \end{Bmatrix} = P.E.(V) \begin{Bmatrix} \sqrt{m_{11}} \\ \sqrt{m_{22}} \\ . \\ . \\ . \\ \sqrt{m_{jj}} \end{Bmatrix} \tag{21}$$

$$V = \beta_{11}\mu_1 + \beta_{12}\mu_2 + \ldots + \beta_{1j}\mu_j \tag{22}$$

$$V = \beta_{12}\left(\frac{\beta_{11}}{\beta_{12}}\mu_1 + \mu_2 + \ldots + \frac{\beta_{1j}}{\beta_{12}}\mu_j \right) \tag{23}$$

This output is a direct measure of shear, or:

$$V = \beta' p_V \tag{24}$$

$$R_A = \left(\frac{\beta_{12}}{\beta_{11}} - 1 \right) R \tag{25}$$

$$V_L = \beta_{11}\mu_1 + \beta_{12}\mu_2 + \beta_{13}\mu_3 + \beta_{14}M_L + \beta_{15}V_R + \beta_{16}M_R + \beta_{17}T_R \tag{26}$$

In matrix notation, the β coefficients are computed by a least squares procedure starting with equation (26)

$$V_L = \lfloor \mu_1\mu_2\mu_3 M_L V_R M_R T_R \rfloor \begin{Bmatrix} \beta_{11} \\ \beta_{12} \\ \beta_{13} \\ \beta_{14} \\ \beta_{15} \\ \beta_{16} \\ \beta_{17} \end{Bmatrix} \tag{27}$$

The preliminary calibration data for the *n* values of applied shears and moments corresponding to the strain gauges response are:

$$\begin{Bmatrix} V'_{L_1} \\ V'_{L_2} \\ . \\ . \\ . \\ V'_{L_n} \end{Bmatrix} = \left\| \begin{matrix} \mu_{11}\mu_{12}\mu_{13} M'_{L_1} V'_{R_1} M'_{R_1} T'_{R_1} \\ \mu_{21}\mu_{22}\mu_{23} M'_{L_2} V'_{R_2} M'_{R_2} T'_{R_2} \\ . \quad . \quad . \quad . \quad . \quad . \quad . \\ . \quad . \quad . \quad . \quad . \quad . \quad . \\ . \quad . \quad . \quad . \quad . \quad . \quad . \\ \mu_{n1}\mu_{n2}\mu_{n3} M'_{L_n} V'_{R_n} M'_{R_n} T'_{R_n} \end{matrix} \right\| \begin{Bmatrix} \beta_{11} \\ \beta_{12} \\ \beta_{13} \\ \beta_{14} \\ \beta_{15} \\ \beta_{16} \\ \beta_{17} \end{Bmatrix} \tag{28a}$$

or

$$\{V'_L\} = \|R\|\{\beta\} \tag{28b}$$

$$\left\{ \|R\|^T \{V'_L\} \right\} = [\|R\|^T \|R\|]\{\beta\} \tag{29}$$

where

$$\{\beta\} = [\|R\|^T \|R\|]^{-1} \left\{ \|R\|^T \{V_L'\} \right\} \tag{30}$$

The coefficients for the preliminary equations for M_T, T_L, V_R, M_R and T_R are obtained in a similar manner from simplified load equations similar to equation 26 and may be summarized in a matrix form as:

$$\begin{bmatrix} V_L & - & - & - & - & - \\ - & M_L & - & - & - & - \\ - & - & T_L & - & - & - \\ - & - & - & V_R & - & - \\ - & - & - & - & M_R & - \\ - & - & - & - & - & T_R \end{bmatrix} = \begin{Vmatrix} \lfloor \mu_1 \ \mu_2 \ \mu_3 \rfloor_{V_L} & |M_L & V_R & M_R & T_R \\ \lfloor \mu_4 \ \mu_5 \ \mu_6 \rfloor_{M_L} & |V_L & V_R & M_R & T_R \\ \lfloor \mu_7 \ \mu_8 \ \mu_9 \rfloor_{T_L} & |M_L & V_R & M_R & T_R \\ \lfloor \mu_{10} \ \mu_{11} \ \mu_{12} \rfloor_{V_R} & |M_R & V_L & M_L & T_L \\ \lfloor \mu_{13} \ \mu_{14} \ \mu_{15} \rfloor_{M_R} & |V_R & V_L & M_L & T_L \\ \lfloor \mu_{16} \ \mu_{17} \ \mu_{18} \rfloor_{T_R} & |M_R & V_L & M_L & T_L \end{Vmatrix} \begin{Vmatrix} \beta_{11} & \beta_{21} & \beta_{31} & \beta_{41} & \beta_{51} & \beta_{61} \\ \beta_{12} & \beta_{22} & \beta_{32} & \beta_{42} & \beta_{52} & \beta_{62} \\ \underline{\beta_{13}} & \underline{\beta_{23}} & \underline{\beta_{33}} & \underline{\beta_{43}} & \underline{\beta_{53}} & \underline{\beta_{63}} \\ \beta_{14} & \beta_{24} & \beta_{34} & \beta_{44} & \beta_{54} & \beta_{64} \\ \beta_{15} & \beta_{25} & \beta_{35} & \beta_{45} & \beta_{55} & \beta_{65} \\ \beta_{16} & \beta_{26} & \beta_{36} & \beta_{46} & \beta_{56} & \beta_{66} \\ \beta_{17} & \beta_{27} & \beta_{37} & \beta_{47} & \beta_{57} & \beta_{67} \end{Vmatrix} \tag{31}$$

Where the terms on the principal diagonal of the left side are the only ones of interest. For example, the attenuation factors for the shear sensitive combined bridge on the left side would be obtained from the equation:

$$\rho_{V_L} = \left(\frac{\beta_{11}}{\beta_{1k}} \mu_1 + \frac{\beta_{12}}{\beta_{2k}} \mu_2 + \frac{\beta_{13}}{\beta_{1k}} \mu_3 \right) \tag{32}$$

The final equation to be used in computing of the flight loads is the following:

$$\begin{Bmatrix} V_L \\ M_L \\ T_L \\ V_R \\ M_R \\ T_R \end{Bmatrix} = \begin{bmatrix} \beta'_{11} & \beta'_{12} & \beta'_{13} & \beta'_{14} & \beta'_{15} & \beta'_{16} \\ \beta'_{21} & \beta'_{22} & \beta'_{23} & \beta'_{24} & \beta'_{25} & \beta'_{26} \\ \beta'_{31} & \beta'_{32} & \beta'_{33} & \beta'_{34} & \beta'_{35} & \beta'_{36} \\ \beta'_{41} & \beta'_{42} & \beta'_{43} & \beta'_{44} & \beta'_{45} & \beta'_{46} \\ \beta'_{51} & \beta'_{52} & \beta'_{53} & \beta'_{54} & \beta'_{55} & \beta'_{56} \\ \beta'_{61} & \beta'_{62} & \beta'_{63} & \beta'_{64} & \beta'_{65} & \beta'_{66} \end{bmatrix} \begin{Bmatrix} \rho_{V_L} \\ \rho_{M_L} \\ \rho_{T_L} \\ \rho_{V_R} \\ \rho_{M_R} \\ \rho_{T_R} \end{Bmatrix} \tag{33}$$

3. NUMERICAL EXPERIMENTS ON THE PHENOMENON OF FATIGUE OF AERONAUTICAL STRUCTURES

The methods for estimating the life span to variable amplitude loading is generally based on constant amplitude test results and they consist of a cycles counting procedure (Rainflow) followed by the determination of the S-N curves and the subsequent application of a damage accumulation rule.

Generally differences were found in both numerical and experimental results and between the numerical results calculated with different methods. Because the results are affected by each component of a general procedure, it is important to know the extent of contribution for each component.

This requires a study to compare some possible methods of predictive calculation and the influence of each step of a procedure over the entire process. The "rain flow" method for cycles counting developed simultaneously by Endo [15] et al. and by Jonge [16], is considered to be the best procedure to determine the events that cause damage in a complex history of fatigue loading.

3.1 Development of the IAR-99 aircraft finite element model (FEM)

Figure 2 shows the geometry of the IAR-99 aircraft general structure and Figure 3 presents the distribution of the fuselage frames according to the theoretic drawing; Figure 4 shows the theoretical models of the lifting surfaces (projections in chords plan).

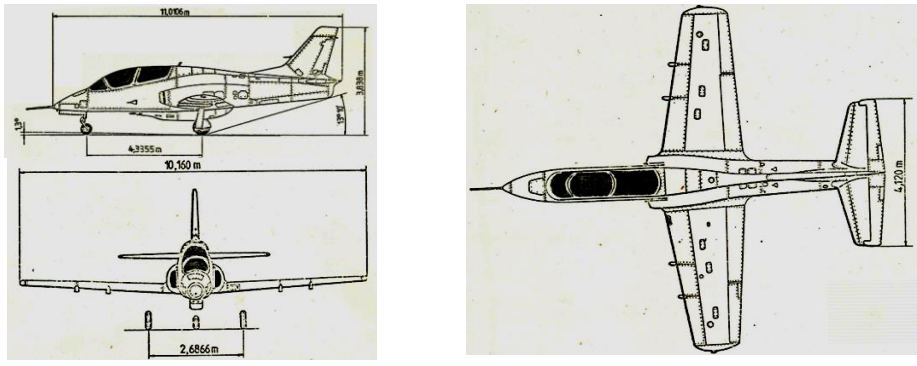

Figure 2. Geometry of the IAR-99 aircraft general structure

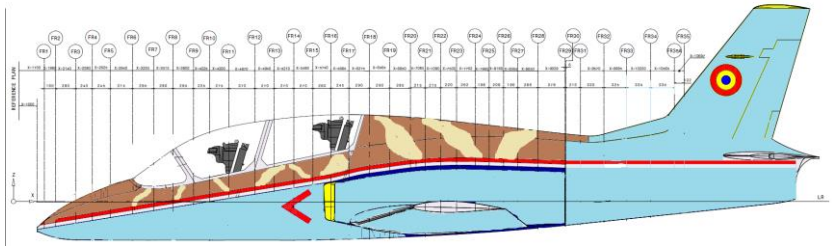

Figure 3. Distribution of the fuselage frames

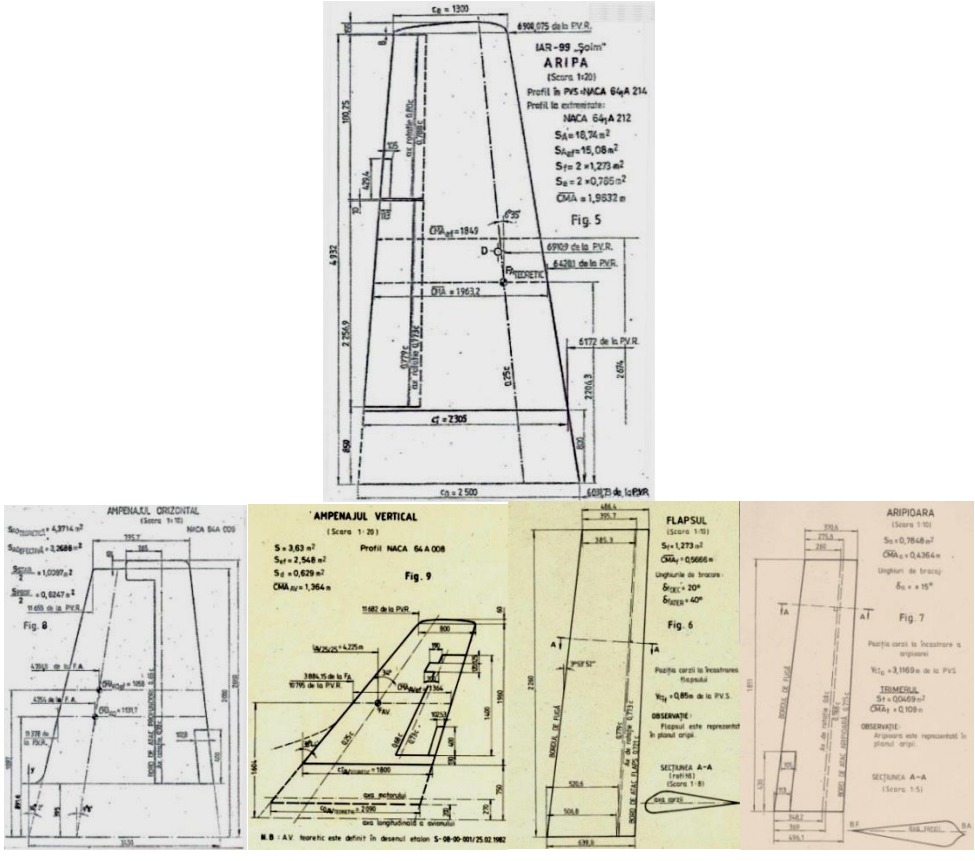

Figure 4. Geometry of the lifting surfaces

CATIA models of the wing fuselage junction are further presented in Figures 5, 6 and 7; subsequently they are imported into PATRAN (Figure 8: the idealized finite element model).

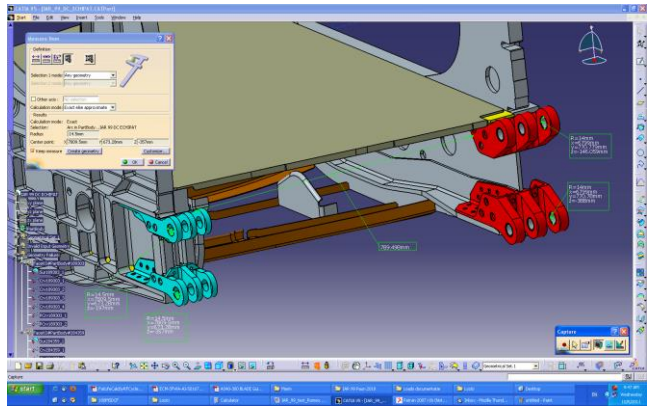

Figure 5. Central fuselage –wing junction assembly (fuselage fittings)

The stress determination on the lower junction fitting was performed using the FEM model in PATRAN/ NASTRAN.

The strain gauges were located on the lower fittings of the wing-fuselage junction for the following reasons: high calculated stress values; elevated recorded stress values in static tests; fitting eye breaking during a fatigue test, easy access to the strain gauges location

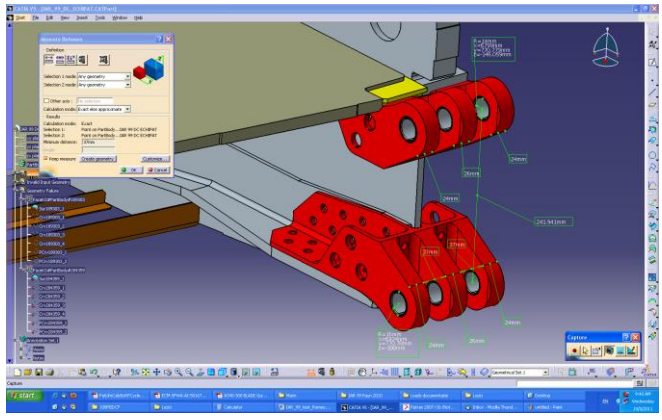

Figure 6. Front, upper and lower fittings, central fuselage C20

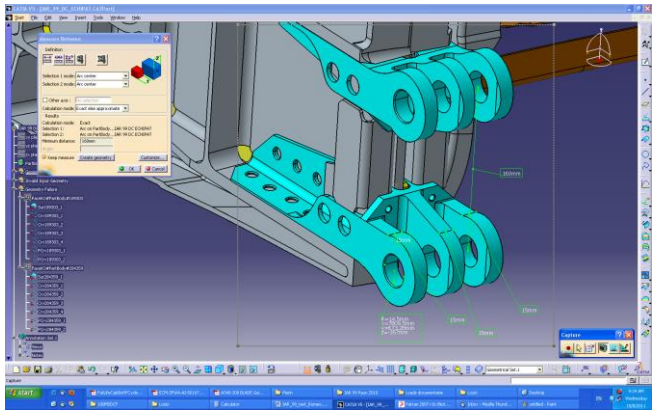

Figure 7. Rear, upper and lower fittings, central fuselage C 24

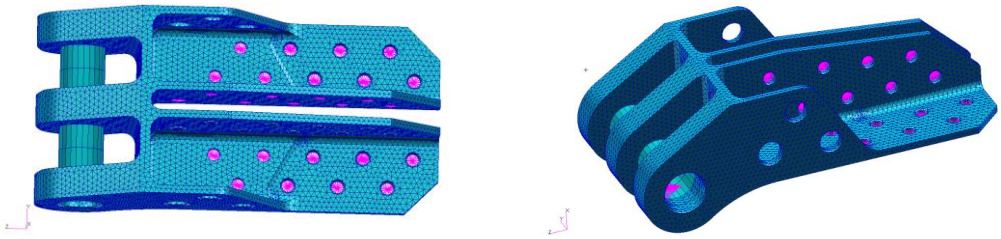

Figure 8. Idealized model of the fuselage lower fittings

Figure 9 shows the distribution of strain gauges on the fittings mesh and the uncalibrated stress state, registered in the FEM model.

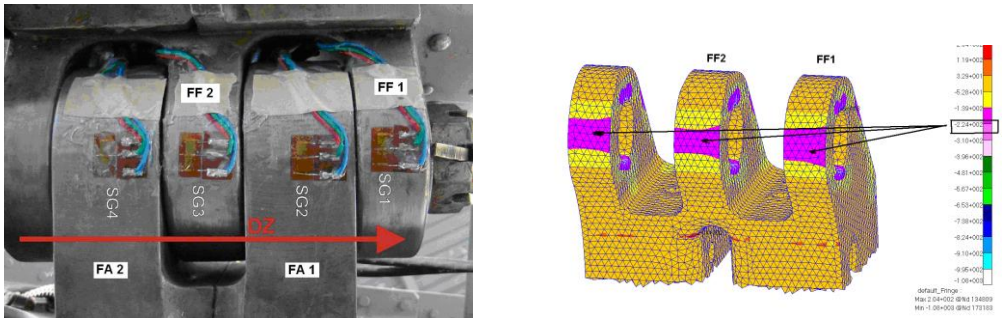

Figure 9. Wing –fuselage lower junction, calculated and instrumented

3.2 Numerical simulation of the static, fatigue and vibration tests using FEM

The numerical simulation of static and fatigue tests consists in developing a FEM model of the item to be tested and applying loadings in a manner similar to the real one. FEM model development in accordance with the real structure (geometry and material modeling) was previously exposed.

To apply loads in the FEM model of the item to be tested (which is also called the test specimen) it is necessary to develop a FEM model, generically called the model of the device needed to achieve the test.

Table 1 and Figures 10 and 11 show the values of the forces, their implementation schedule and a detail of the finite element model for the static test of the wing - fuselage junction.

Table 1. Forces applied to the wing-fuselage junction during the static test

Yoke no	Wing chord	LP caisson chord	XLA 0.293C	XLP	XBA	Force aplied on the yoke [Kgf}
1	2276	1570	667	1263	307	1469
3	2102	1450	616	1409	(41)	920
4	2026	1398	594	865	533	1270
5	1944	1341	570	1108	233	903
6	1894	1307	555	1059	248	1040
7	1791	1236	525	(638)	598	501
8	1735	1197	508	738	459	403
9	1675	1156	491	794	362	803
10	1627	1123	477	762	361	1256
11	1533	1058	449	715	343	855
12	1425	983	418	641	342	618
13	1310	904	384	-63	967	40

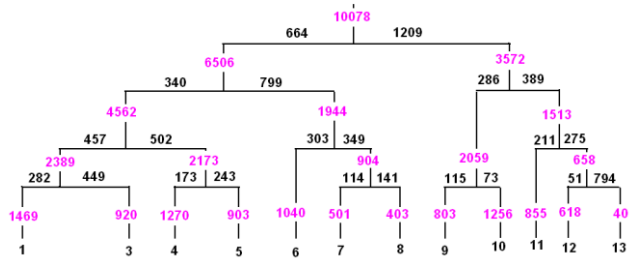

Figure 10. Forces applied to the wing-fuselage junction during the static test

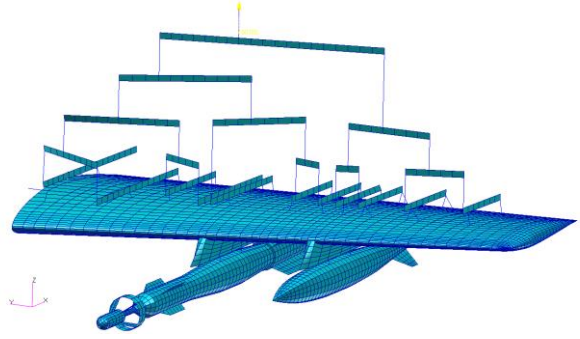

Figure 11. FEM detail of the central fuselage-wing junction during the IAR-99 aircraft static test

4. PHYSICAL FATIGUE EXPERIMENTS OF AERONAUTICAL STRUCTURES

On 30.09.2011, IAR-99 Hawk no 718 performed its first flight at the IN FLIGHT RESEARCH & TEST CENTER, CCIZ.Craiova. The aircraft was equipped with a flight data recorder. The information collected in the seven flights were used in the present work to monitor the running life of IAR 99 aircraft.

The meanings and measurement units of the in-flight registered parameters are:

1. Tamb — ambient temperature – Celsius degrees
2. Nanalogic — engine speed -%
3. Qc — flow rate of fuel - l/h
4. CAS_1553B — calibrated speed - Km/h
5. Norm_accl_1553B — Nz
6. Pickle_1553B — evolution marker
7. Pich_1553B — dive angle - degrees
8. Pich_R_1553B — angular velocity of pitching - degrees/sec
9. ROLL_1553B — roll angle - degrees
10. ROLL_R_1553B — roll angular velocity - degrees/sec
11. TRUE_HDG_1553B — heading-degrees
12. YAW_R_1553B — yaw angular velocity - degrees/sec
13. ALT_HBC — barometric altitude - m
14. AOA_TRUE_1553B — angle of incidence-degrees
15. SG1-4 4 microstrain strain gauge bridge signals
16. FUEL_QANT_1553B Instantaneous fuel amount that allows calculating the instantaneous weight of the aircraft Gav=0,803*FUEL_QANT_1553B+3865 Kg (the relationship is deduced from the aircraft weighing).

17. The raw output (gross) of a numerical experiment consists of an Excel file that contains a matrix with 16 columns corresponding to registered parameters and a variable number of lines linked to the event duration. For example, for a flight of half an hour, during which all the 19 parameters described above were recorded with a frequency of 4 s^{-1}, the matrix contains 136800 values. We chose this method of the numerical experimental results management due to its simplicity and outstanding flexibility.

If an Excel "page" is dedicated to a flight, on that page you can simply draw time variation diagrams of any parameter for the entire flight range or for specific areas of interest. The derivatives calculation of the recorded values is reduced to dividing successive differences of a parameter (P_{i+1}-P_i) at the corresponding temporal step (T_{i+1}-T_i) thus Deriv(P)= (P_{i+1}-P_i)/ (T_{i+1}-T_i). Obviously the accuracy depends on the temporal step of reading and is satisfactory for steps <sec^{-1}. Figure 12 presents a screenshot of an Excel page, including the parameter values and some flight charts.

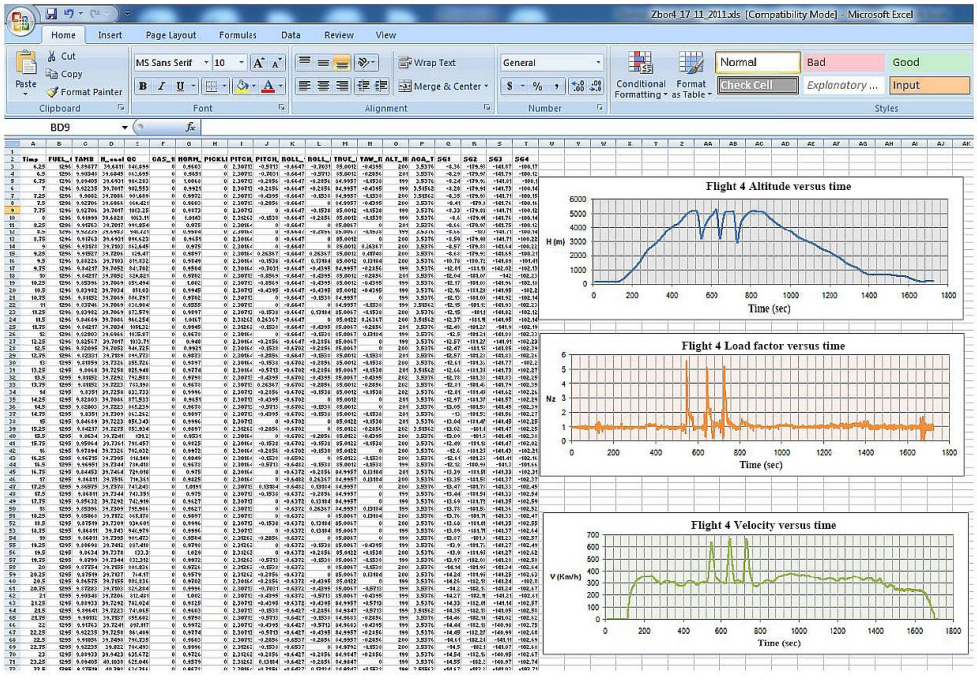

Figure 12. Screen capture of the fatigue monitoring software for IAR-99

Various procedures for recorded parameters processing with numerical examples associated to IAR-99-718 will be detailed next. Experimental flight profiles can be determined on the basis of the in -flight records for various parameters such as altitude, speed, load factor, incidence, etc. Figure 4.2.1 presents a record of the IAR 99 altitude evolution, in a mission called "Flight 4". The duration of the mission was approximately of 30 minutes, with 1700 seconds of actual recording. The plane took off from second zero, made a plateau at a height of 200 m for 3 minutes and then climbed to the height of 5000 m within 8 minutes. Then the plane executed for about seven minutes, three relatively similar evolutions consisting of dives up to 3000 m, followed by pull-out (resource) and return to 5000 meters altitude. The flight ended after 10 minutes of descent and a plateau up to the landing. The digital recording of the altitude variation with time was performed with a frequency of reading at 250 milliseconds.

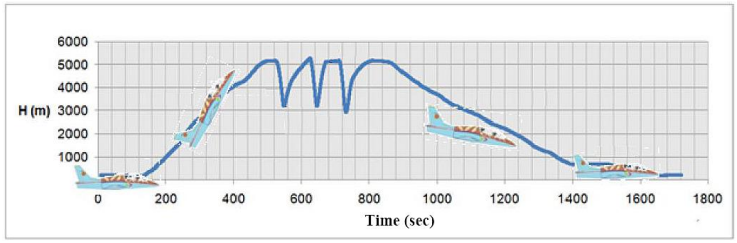

Figure 13. Flight 4 – Altitude versus time

As seen in Figure 13, the slopes of the climb, descent and dive can be considered as being relatively constant for a type of evolution in which case the aircraft rate of climb can be determined. For example, for a climbing from H_1 = 0 to H_2 =5000m, which lasted from T_1 = 150s up toT_2 = 500 s, the average rate of climb of the aircraft was 14.3 m / s while for a dive from 5000 m to 3000 m, which lasted for 20s the average rate of descent of the aircraft was 100 m / s. For a more accurate calculation, a diagram of the recorded parameter, in this case the altitude can be drawn, at the appropriate temporal scale or the recorded numeric values can be used. The same mission (Flight 4) is detailed in figure14 in the time interval ranging from T_1= 500 s to T_2 = 800 s. It can be seen that the pull-out takes about five seconds, or a ground attack with a dive from 5000 m to 3000 m, followed by a pull-out and release back to 5000 m, takes less than 30 seconds

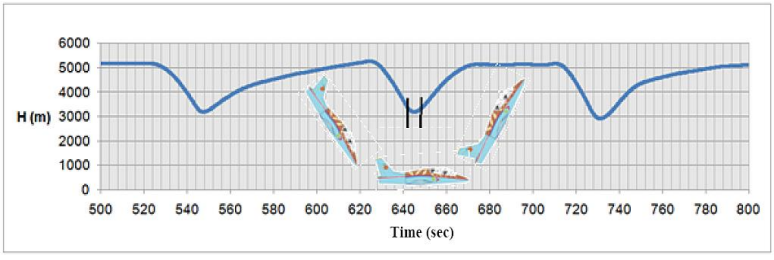

Figure 14. Flight 4 EXPERIMENT - Diagram of the flight altitude (detail)

Figure 15 and Figure 16 present the diagrams of the calibrated speed variation during the entire flight and during the interval of time ranging between T_1 = 500 sec and T_2 = 800sec, respectively.

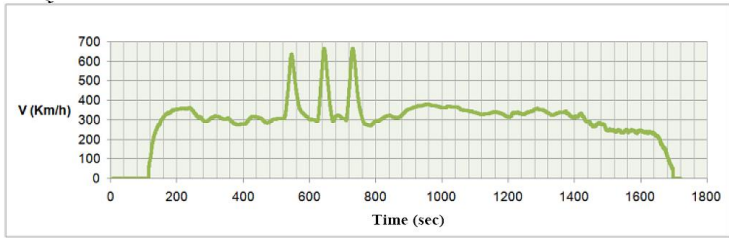

Figure 15. Flight 4 EXPERIMENT - Diagram of the flight speed

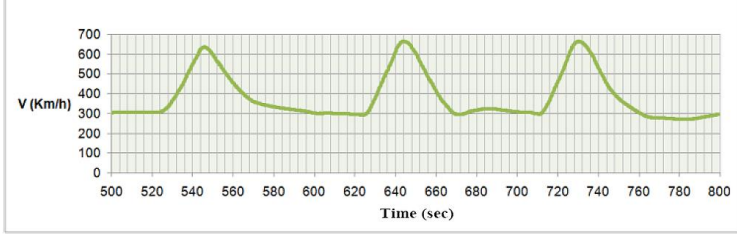

Figure 16. Flight 4 EXPERIMENT - Diagram of the flight speed (detail)

Fig. 17 and Fig. 18 present the diagrams of the variation of fuel consumption during the entire flight and during the interval of time ranging between T1 = 0 sec and T2 = 900sec, respectively.

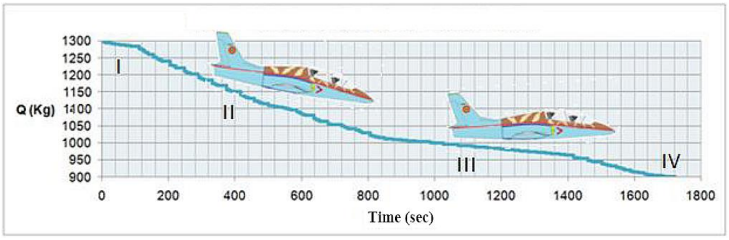

Figure 17. Flight 4 EXPERIMENT - Diagram of fuel consumption

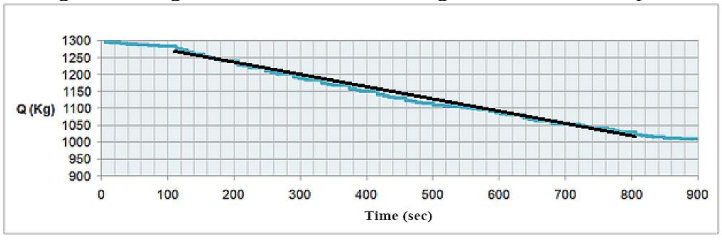

Figure 18. Flight 4 EXPERIMENT - Diagram of the constant fuel consumption (detail)

By visual inspection four main areas of specific fuel consumption, q, relatively constant were identified

Zona I	T=0 - 120 sec	Q=1300-1280 Kg	q=0.166 Kg/sec
Zona II	T=120 - 820 sec	Q=1280-1000 Kg	q=0.4 Kg/sec
Zona III	T=820 - 1400 sec	Q=1000-950 Kg	q=0.086 Kg/sec
Zona IV	T=1400 - 1700 sec	Q=950-900 Kg	q=0.166 Kg/sec

Figure 19 and Figure 20 present the diagrams of the variation in incidence during the entire flight and during the interval of time ranging between T_1 = 500 sec and T_2 = 800sec, respectively.

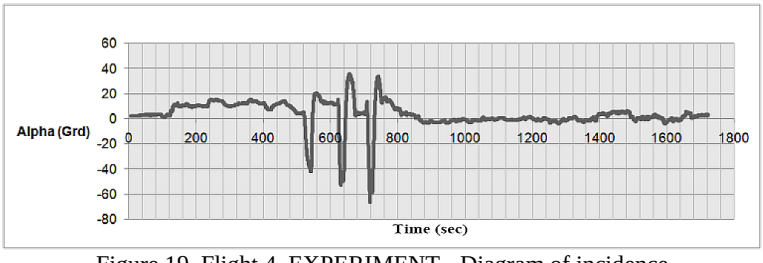

Figure 19. Flight 4 EXPERIMENT - Diagram of incidence

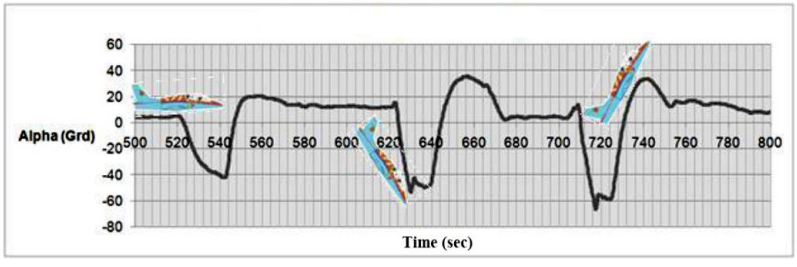

Figure 20. Flight 4 EXPERIMENT - Diagram of incidence (detail)

The maximum positive incidence is of 38 degrees and the minimum negative value is -60 degrees. Figure 21 and Figure 22 present the diagrams of the vertical load factor variation

during the entire flight and during the interval of time ranging between T1 = 500 sec and T2 = 800sec, respectively.

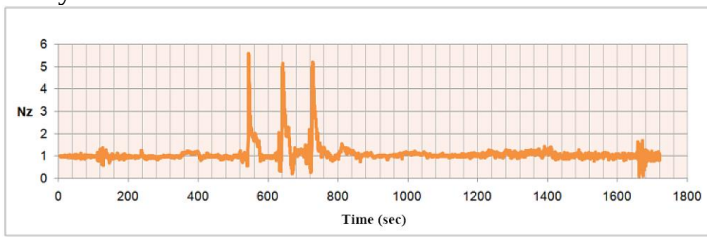

Figure 21. Flight 4 EXPERIMENT - Diagram of the vertical load factor

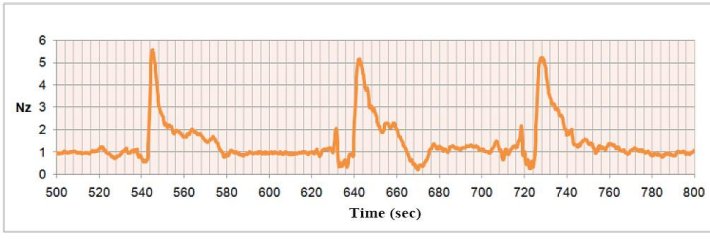

Figure 22. Flight 4 EXPERIMENT - Diagram of the vertical load factor (detail)

Positioning of strain gauges in the wing central fuselage junction is shown in Figure 23. As the wing-fuselage junction is symmetrical both on the front and rear and on the left and right in Figure 24 is also indicated the flight direction DZ. Strain gauges SG 1 and SG 3 are located on the fuselage fittings FF1 and FF2, respectively and strain gauges SG 2 and SG 4 are located on the wing fittings FA1 and FA2, respectively.

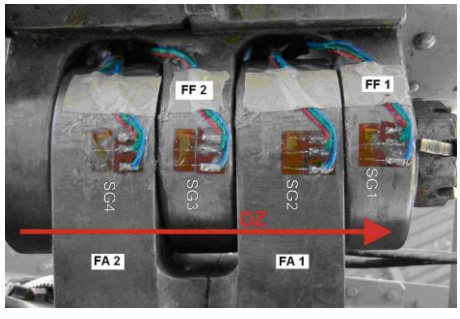

Figure 23. Flight 4 Instrumented wing - fuselage lower junction

Figures 24 to 27 show the diagrams of the strain gauges SG1 to SG4 during the entire flight

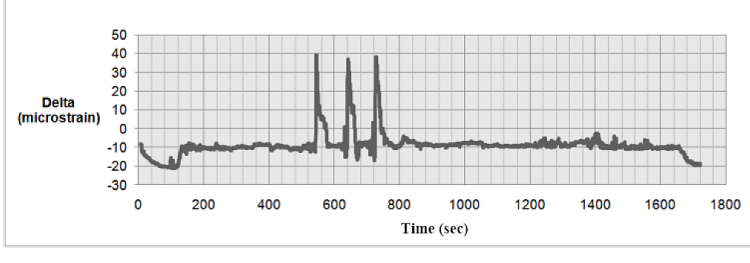

Figure 24. Flight 4 EXPERIMENT - Diagram of the strain gauge SG 1

The tensions in fittings are proportional to the modulus of elasticity of the material on which the fittings are stuck (steel E = 210 000 MPa) and they occur as a result of the calibration process.

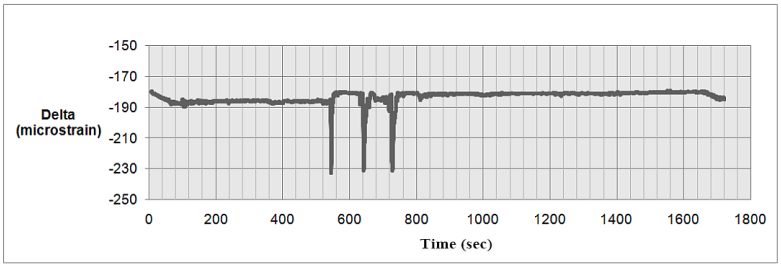

Figure 25. Flight 4 EXPERIMENT - Diagram of the strain gauge SG 2

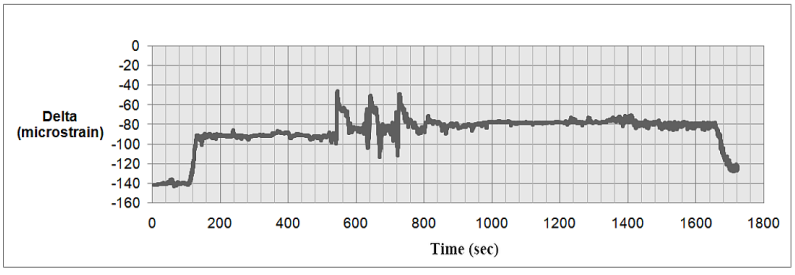

Figure 26. Flight 4 EXPERIMENT - Diagram of the strain gauge SG 3

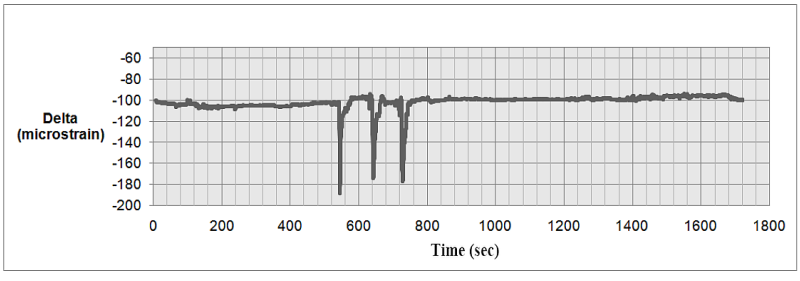

Figure 27. Flight 4 EXPERIMENT - Diagram of the strain gauge SG 4

3 maximums of micro-deformations can be qualitatively observed in points corresponding to the 3 factors of maximum load, touched during the pull-out of the 3 dives from 5000m to 3000m.

5. CONCLUSIONS AND CRITICAL ANALYSIS OF THE NUMERICAL AND EXPERIMENTAL RESULTS

A theoretical flight profile, also called a flight plan or mission, is an array of quantitative and mainly qualitative information, leading to fulfilling that mission. For example, a mission of interception may be based on a theoretical flight profile consisting of the following phases and associated requirements:

Phase	Examples of extreme or optimal quality requirements
1. TAXIING	Minimum distance, Minimum time, Maximum Speed
2. TAKE-OFF	Minimum distance, Minimum time, Minimum Speed
3. PLATEAU	Maximum acceleration
4. CLIMB	Maximum rate of climb
5. CRUISE	Maximum calibrated speed, Maximum or Minimum altitude
6. ATTACK	Maximum rate of descent, Minimum time
7. CLEARING	Maximum rate of climb, Maximim load factor

8.	RUNNING	Maximum calibrated speed, Maximum or Minimum altitude
9.	DESCENT	Optimim rate of descent, Miminum fuel consumption
10.	PLATEAU	Maximum deceleration, Minimum distance, Minimum altitude
11.	LANDING	Minimum distance, Minimum time, Minimum Speed
12.	TAXIING	Minimum distance, Minimum time

Based on the study of the aircraft performance, the quality requirements may be accompanied by quantitative requirements usually associated to operational maneuver diagrams and ambient conditions existing at the time. The development of a flight plan can be also seen as a problem of constrained optimum. Fulfilling the mission in minimum time can be chosen as a target function; the optimization variables are: the distance, speed, altitude and associated time. The constraints are mainly represented by the extreme values of the performances of the interceptor but also of the air enemy. In other words, if the performances of the target plane are superior to those of the interceptor, the optimal problem can be divergent (it has no solutions). For civil aircraft the flight profile may be considered as derived from the military profile by eliminating the specific phases: 6 - ATTACK. 7 - CLEARING and 8 - RUNNING.

REFERENCES

[1] *** ANSYS User's Manual for Revision 5.0 – Volume I, II, III, IV.

[2] *** AvP-970- Design Requirements for Service Aircraft, vol. **I**. Airplane Design Requirements, 1975.

[3] *** MIL-F-8785 (ASG), Military Specification-Flying Qualities of Piloted Airplanes, 1969.

[4] *** C-2205/ 06.1999, *Model idealizare structura pentru estimarea duratei de viata a structurii avionului IAR-99*, INCAS Paper.

[5] J. Wright, J. Cooper, *Introduction to Aircraft Aeroelasticity and Loads***,** John Wiley & Sons, Ltd., 2007.

[6] D. P. Raymer, *Aircraft Design. A conceptual Approach.* AIAA Education Series, 1992.

[7] D. Lozici-Branzei, D. Baran, S. Tataru, Flutter Analysis of the IAR-99 SOIM aircraft, *INCAS Bulletin*, volume **5**, Issue 2, (online) ISSN 2247–4528, (print) ISSN 2066–8201, ISSN–L 2066–8201, DOI: 10.13111/2066-8201.2013.5.2.5, pp. 33-43, 2013.

[8.] D. Dinca Baran, Mathematical Models Used in Studying the Chaotic Vibration of Buckled Beams, *Mechanics Research Communications*, Vol. **21**, Issue 2, March-April, pp. 189-196, 1994.

[9]. D. Baran, M. Stere, S. Tataru, D. Lozici-Branzei, N. Apostolescu, R. Bisca, B. Caloian, Design&Analysis Tools and Techniques for Aerospace Structures in a 3D Environment, *INCAS Bulletin*, Volume **1**, no. 1, (online) ISSN 2247–4528, (print) ISSN 2066–8201, ISSN–L 2066–8201, DOI: 10.13111/2066-8201.2009.1.1.17, pp. 93-95, 2009.

[10]. S. Tataru, D. Lozici-Branzei, D. Baran, M. Stere, Predictive Assessment of an Aircraft Structure Behaviour, *INCAS Bulletin*, Volume **1**, no 2, (online) ISSN 2247–4528, (print) ISSN 2066–8201, ISSN–L 2066–8201, DOI: 10.13111/2066-8201.2009.1.2.18, pp. 129-135, 2009.

[11] Dorin Lozici-Brinzei, Simion Tataru, Radu Bisca, *IAR-99 Ground Vibration Tests and Dynamics, Finite Element Model* -AFASES 2011.

[12] D. Lozici-Brinzei, R. Bisca, S. Tataru, Loads in the Design of Flight Vehicles, *INCAS Bulletin*, Volume **2**, no 3, (online) ISSN 2247–4528, (print) ISSN 2066–8201, ISSN–L 2066–8201, DOI: 10.13111/2066-8201.2010.2.3.6, pp. 51-59, 2010.

[13] D. Baran, D. Lozici-Brinzei, S. Tataru, Dynamic study of the virtual prototype of the IAR-99 SOIM Aircraft, *INCAS Bulletin*, Volume **5,** Issue 3, (online) ISSN 2247–4528, (print) ISSN 2066–8201, ISSN–L 2066–8201, DOI: 10.13111/2066-8201.2013.5.3.1, pp. 3-11, 2013.

[14] S. Tataru**,** D. Baran, D. Lozici-Brinzei, Advanced Techniques of Stress Analysis *INCAS Bulletin*, Volume **5,** Issue 4, (online) ISSN 2247–4528, (print) ISSN 2066–8201, ISSN–L 2066–8201.

[15] T. Endo, M. Matsuishi, *The Rainflow Method in Fatigue –the Tatsuo Endo Memorial Volume*, Murakami Y. (Ed)., ISBN 0-7506-0504-9, July, 1991.

[16] J. B. de Jonge, *The analysis of load-time histories by means of counting methods', in 'Helicopter Fatigue design guide*, F. Liard (ed.)., AGARD-AG-292, November, 1983.